Journal of the European Ceramic Society 40 (2020) 4436–4444

Contents lists available at ScienceDirect

Journal of the European Ceramic Society

journal homepage: www.elsevier.com/locate/jeurceramsoc

Original Article

Oxidation behaviour of V_2AlC MAX phase coatings

Clio Azina[a,b,*], Stanislav Mráz[b], Grzegorz Greczynski[a], Marcus Hans[b], Daniel Primetzhofer[c], Jochen M. Schneider[b], Per Eklund[a]

[a] Thin Film Physics Division, Department of Physics, Chemistry and Biology (IFM), Linköping University, SE-58183 Linköping, Sweden
[b] Materials Chemistry, RWTH Aachen University, Kope. 10, D-52074, Aachen, Germany
[c] Department of Physics and Astronomy, Uppsala University, Lägerhyddsvägen 1, S-75120, Uppsala, Sweden

ARTICLE INFO

Keywords:
MAX phases
Coatings
Oxidation
V_2AlC

ABSTRACT

We report on the oxidation behaviour of V2AlC coatings up to 800 °C, in air. The coatings were deposited at 580 °C using magnetron sputtering from a powder metallurgical composite V2AlC target and were subsequently oxidised for 5, 15 and 30 min. The microstructural evolution of the samples was investigated, and X-ray diffraction patterns were collected to track the formation of oxides. The first indications of oxidation appear after just 15 min at 500 °C, as V-based oxides grew on the surface of the coatings. Later, the presence of mostly V-based oxides and ternary (V, Al)-oxides was observed starting after 5 min at 600 °C. Further analyses confirmed outward diffusion of V and inward diffusion of O, while Al tends to sublimate. α-Al2O3 was only indexed after 5 min at 800 °C. Ex-situ electrical resistivity measurements allowed tracking the oxidation progress of the V2AlC coating.

1. Introduction

V_2AlC belongs to the class of $M_{n+1}AX_n$ phases, where M is an early transition metal, A is an element primarily from groups 13–16, and X is carbon and/or nitrogen, with n = 1, 2 or 3. [1–3] MAX phases are nanolaminated ternary carbides/nitrides that crystallize in hexagonal structures composed of $M_{n+1}X_n$ layers interleaved with atomic layers of A-element. These materials are being considered for a variety of applications because of their unique, hybrid metal/ceramic properties, resulting from their structure and atomic arrangement. [3,4] More specifically, MAX phases are considered for applications in extreme environments as they exhibit remarkable thermal stability and oxidation resistance.

The context of the present study is the development of accident-tolerant fuel (ATF) cladding materials for Gen-II/III light water reactors (LWR), where MAX phases are considered for coatings on the conventionally used zircaloys. V_2AlC is selected because of its relatively low deposition temperature and good irradiation tolerance [5].

Thermal stability and oxidation resistance are of utmost importance for materials intended for extreme environment applications. The thermal stability of common MAX phases such as Ti_2AlC, Ti_3AlC_2, Cr_2AlC and Ti_3SiC_2 have been widely discussed in the literature. [6–10] Ti-based MAX phases are reported to be affected by decomposition at temperatures above 1400 °C, mostly because of sublimation of A-element and eventually Ti [10]. Hajas et al. have studied the thermal stability of Cr_2AlC and have observed first traces of Cr_3C_2 and Cr_7C_3 at 1320 °C, indicating the beginning of decomposition through Al depletion. [11] Furthermore, Cr_2AlC melts incongruently at a temperature of about 1500 °C. [12] Contrarily, Xiao et al. reported that Cr_2AlC could be stable up to 1500 °C, after which point it decomposes into Al_8Cr_5 and $Cr_{23}C_6$. [13]

In comparison, few studies have focused on the thermal stability of V_2AlC. Kulkarni et al. have investigated the thermal stability of bulk V_2AlC up to 950 °C in Ar and did not report any phase transformation or decomposition. [14] Furthermore, it has been shown that temperatures as high as 850 °C assist in the crystallization and further atomic arrangement within V_2AlC coatings deposited at lower temperatures. [15]

During thermal treatment of MAX phases in vacuum or in an inert environment, the weakly bonded A-elements diffuse within the structure and, depending on the temperature, may lead to sublimation of the A-elements. [16] In the case of an oxidising environment, however, it has been shown that MAX phases can be passivated with an oxide layer. Indeed, the A-element tends to form a dense oxide scale on the surface, limiting hence, the inward diffusion of O^{-2}. Therefore, it is the interfacial region, between the coating and the formed oxide layer, that is first affected by decomposition. [17]

A representative example is the case of Cr_2AlC oxidised in air up to 1410 °C. [18–23] The oxidation mechanism follows a parabolic rate law

* Corresponding author at: Thin Film Physics Division, Department of Physics, Chemistry and Biology (IFM), Linköping University, SE-58183 Linköping, Sweden.
E-mail addresses: clio.azina@liu.se, azina@mch.rwth-aachen.de (C. Azina).

https://doi.org/10.1016/j.jeurceramsoc.2020.05.080
Received 29 April 2020; Received in revised form 28 May 2020; Accepted 29 May 2020
Available online 31 May 2020

and is described by inward diffusion of O^{-2} and outward diffusion of Cr^{2+} and Al^{3+}. However, because of the stronger Cr-C bonds, Al oxidises preferentially. This process leads to the formation of a Cr-containing Al_2O_3 scale and an Al-depleted Cr_7C_3 interfacial zone, although Cr_3C_2 has also been reported. On the contrary, Ti-based MAX phases do not exhibit the same behaviour as Cr_2AlC although they also follow a parabolic oxidation rate law. The major difference is that decomposition related to Al-depletion is not as instant as for Cr_2AlC, which is related to the stability of Ti_2AlC down to a $Ti_2Al_{0.5}C$ sub-stoichiometry. [24] High temperature oxidation up to 2000 °C led to selective oxidation of Al and Ti. Cui et al. have reported the early stages of Ti_2AlC oxidation at 900 °C where they showed that after 1 h the cross-section is represented by three zones: the MAX phase, the Al-depleted region and the oxide scale. The scale consisted of an outer TiO_2-rich layer and an inner Al_2O_3-rich one, explained by the faster outgrowth of TiO_2. [25] It is yet important to note that several factors can and will affect the oxidation of a MAX phase. Recent work from Xu et al. has shown that the oxidation of a textured Ti_3AlC_2 MAX phase ceramic is highly anisotropic [26], while Yu et al. discussed the influence of grain size [27].

The oxidation behaviour of V_2AlC was reported by Gupta and Barsoum in 2004. Significant weight gain was reported after close to 2 h at 700 °C and was related to the formation of oxides. [28] The authors investigated the layers included in the formed oxide scale and were able to conclude on the inward diffusion of O ions, while the contributions of V and Al remained unclear. No decomposition was observed as the maximum temperature was set to 700 °C, at which several molten V-based oxides were identified. In 2017, Wang et al. reported on the oxidation resistance of porous V_2AlC, produced by the molten salt method, and have reached similar conclusions. [29]

In this study, coatings obtained by direct current magnetron sputtering from a powder metallurgical composite V_2AlC target were studied. The coatings were oxidised in air in order to conclude on the early stages of oxidation. The effects of temperature and oxidation duration on phase formation and surface morphology were evaluated using X-ray diffraction (XRD) and electron microscopy (SEM). Further chemical composition analyses were carried out in order to conclude on the role of each species during oxidation. The electrical resistivities of the coatings with respect to oxidation time and temperature were also collected.

2. Experimental procedure

A powder metallurgical composite V_2AlC target (Plansee Composite Materials GmbH, Germany) 500 × 88 mm^2 was used to deposit the V_2AlC coatings onto 10 × 10 mm^2 MgO(100) substrates (Crystal GmbH, Germany). The depositions were carried out using an industrial magnetron sputtering system CemeCon CC800/9 (CemeCon AG, Germany). The substrates were located at a distance of 75 mm from the target and were heated to 580 °C as measured with external thermocouples. The base pressure prior to deposition was below 3×10^{-4} Pa. The Ar flow was set to 475 sccm leading to a working pressure approximately 0.9 Pa. The target was kept at a constant DC power of 1000 W. All depositions were 60 min-long and resulted in 3.4 μm-thick coatingss.

The pristine coatings were oxidised in an open furnace. The oxidation temperatures were set to 400, 500, 600, 700 and 800 °C, and were attained with a rate of 10 K/min. The oxidation times were 5, 15 and 30 min. The samples were cooled down at a higher rate to limit additional diffusion and oxidation due to slow cooling.

The structural properties of the deposited coatings were investigated by means of X-ray diffraction (XRD) using a standard θ-2θ geometry in a Panalytical X'pert MRD with Cu K_α radiation. Density measurements were carried out using X-ray reflectivity (XRR) in a Panalytical Empyrean MRD system also equipped with a Cu K_α source. Coating thicknesses and microstructural observations were carried out using scanning electron microscopy (SEM; Zeiss Leo 1550 Gemini).

The electrical resistivities of pristine and oxidised samples were obtained by measuring the sheet resistance with a four-point probe (Jandel RM3000) and then multiplying it by the total coating thickness (in the case of oxidised coatings the total thickness includes the coating and the oxide scale).

Chemical composition depth profiling was carried out by elastic recoil detection analysis (ERDA) at the Tandem Laboratory at Uppsala University. The projectiles were $^{127}I^{8+}$ ions with a primary energy of 36 MeV. Time-energy coincidence spectra were recorded by combination of a time-of-flight setup with a solid state detector [30]. Depth profiles were obtained with the CONTES software package [31]. In order to evaluate the uncertainties of the light elements, a Cr_2AlC reference sample [32] as well as a sapphire (0001) substrate were analyzed in addition to the V_2AlC coatings. The C concentrations were corrected based on the Cr_2AlC reference and systematic uncertainties in the quantification of C and O were 5 and 2% relative deviation, respectively.

XPS core-level spectra were acquired in an Axis Ultra DLD instrument from Kratos Analytical (UK) with the base pressure during spectra acquisition better than 1.1×10^{-9} Torr (1.5×10^{-7} Pa). Monochromatic Al Kα radiation ($h\nu$ = 1486.6 eV) was used and the anode power was set to 150 W. Spectra were obtained at normal emission angle and with the charge neutralizer. The binding energy scale was first calibrated to the Fermi energy cut-off of the sputter-cleaned polycrystalline Ag film and all spectra are presented "as recorded". This was done to avoid uncertainties related to using the C 1s signal from adventitious carbon as the charge reference [33,34], The analyser pass energy was set to 20 eV, which yields the full width at half maximum of 0.55 eV for the Ag $3d_{5/2}$ peak. Spectra were recorded from as-grown samples as well as after several cycles of sputter-etching with 0.5 keV Ar^+ ions incident at an angle of 70° with respect to the sample normal and with the beam rastered over a 3 × 3 mm^2 area. Low ion energy and shallow incidence angle were used to reduce the influence of the sputter-damage on core level spectra [35,36]. The area analysed by XPS was 0.3 × 0.7 mm^2 and centred in the middle of the ion-etched crater. Spectra deconvolution and quantification was performed using CasaXPS software package and sensitivity factors supplied by instrument manufacturer.

Finally, thin lamellae were prepared by focused ion beam (FIB) techniques for microstructural characterisation using scanning transmission electron microscopy (STEM; FEI Helios Nanolab 660) with a STEM III detector. Cross-section energy dispersive X-ray spectroscopy (EDX) line scans were acquired using an EDAX system with an Octane Elect detector. The acceleration voltage and step size of the line scan were 12 kV and 50 nm, respectively.

3. Results and discussions

The XRD patterns collected from the pristine coating and those oxidised for 5, 15, and 30 min at 400, 500, 600, and 700 °C are presented in Fig. 1. No major difference can be observed for the coatings oxidised at 400 and 500 °C (Fig. 1 (a)), which exhibit the V_2AlC MAX phase contributions (PDF: 01-077-3986). However, after 5 min at 600 °C, traces of the first secondary phase can be observed, which has been indexed as VO_2 (PDF: 00-042-0876). After 15 min at 600 °C, V_2O_5 is formed with characteristic peaks appearing at 2θ of ∼ 15° (110), ∼ 21° (200), between 30 and 35° and at ∼ 51° (PDF: 00-041-1426). At 30 min, the increase in intensity of the VO_2 and V_2O_5 contributions can be noticed. After 5 min at 700 °C, the formed phases are VO_2 and V_2O_5, similar to the coating oxidised for 30 min at 600 °C, although their intensities vary, and V_3O_5 (PDF: 00-038-1181). After 15 min at 700 °C, the MAX phase contributions are completely absent which indicates the complete oxidation of the coating. The oxidation is even more evidenced by a change in appearance of the coating as shown in Fig. 2 (d). Indeed, up to 5 min at 600 °C, the coatings have a mirror-like appearance, up to 5 min at 700 °C the coatings become darker and opaque,

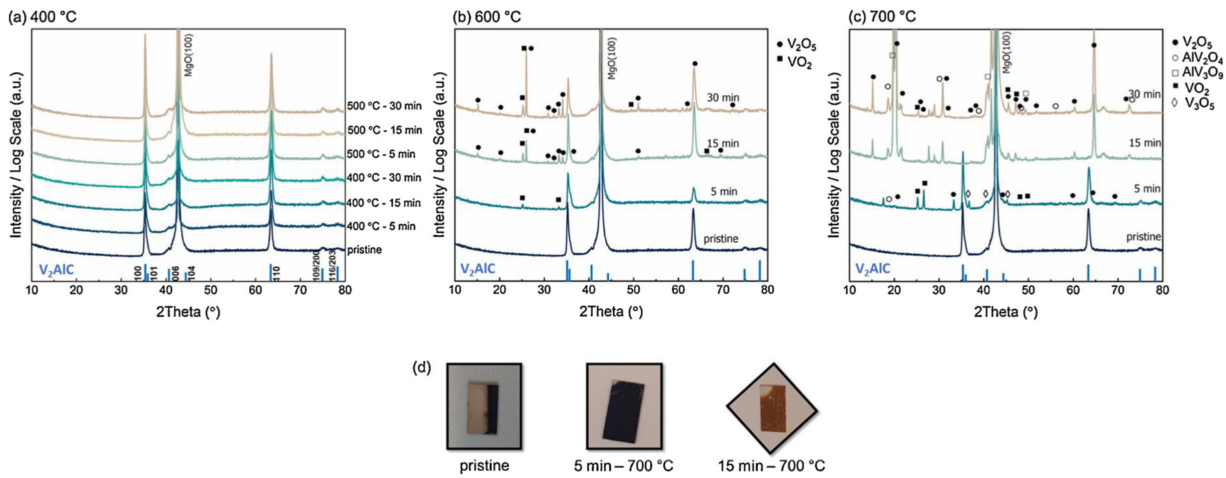

Fig. 1. XRD patterns of as deposited coatings (noted as pristine in figure) and oxidised coatings after 5, 15, and 30 min at (a) 400, (b) 500, (c) 600 and (d) 700 ˚C. (e) Photographs of coating appearances.

while from 15 min at 700 ˚C the coatings exhibit a red to orange colour. The oxides formed after oxidation for 15 and 30 min at 700 ˚C were V_2O_5, VO_2 and the metastable, ternary oxides: AlV_3O_9 (PDF: 00-049-0694) and AlV_2O_4 (PDF: 01-077-2131). All oxides formed at these times and temperatures are V-based and mostly stable [37]. The absence of alumina can be explained by sublimation of Al, as will be shown later. Another possibility could be the formation of amorphous alumina; however, this possibility was not supported by XPS and ERDA observations.

The XRD pattern and corresponding SEM micrographs of the coating oxidised for 5 min at 800 ˚C are given in Fig. 2. One can notice that the MAX phase has been completely oxidised, as none of the initial MAX phase contributions ((Fig. 2 (a)) can be observed. The oxides formed were $AlVO_3$ (PDF: 00-025-0027), $AlVO_4$ (PDF: 00-039-0276), V_8O_{15} (PDF: 00-018-1448), V_2O_3 (PDF: 00-034-0187), V_3O_5, V_2O_5 and VO_2. Interestingly, α-Al_2O_3 was also indexed (PDF: 00-046-1212), which was not observed at lower temperatures. Furthermore, both metastable phases AlV_3O_9 and AlV_2O_4 that were observed at 700 ˚C were not detected at 800 ˚C. We conclude that, since $AlVO_4$ is the only stable ternary oxide in the Al-V-O system, [38] the metastable phases decomposed at 800 ˚C. Indeed, AlV_2O_4 is known to decompose into Al_2O_3, V_2O_3 and V, [39] while AlV_3O_9 can decompose into V_2O_5 and $AlVO_4$, [40] explaining, hence, the presence of the ternary and V_2O_3 at a higher temperature. As for $AlVO_3$, which decomposes into Al_2O_3 and V_2O_3, the

Table 1
Summary of detected phases with respect to oxidation time and temperature.

Time (min)	400 ˚C	500 ˚C	600 ˚C	700 ˚C	800 ˚C	
5	V_2AlC	V_2AlC	V_2AlC VO_2	V_2AlC VO_2 V_2O_5	VO_2 V_2O_5 V_3O_5 V_8O_{15}	V_2O_3 $AlVO_4$ $AlVO_3$* Al_2O_3
15	V_2AlC	V_2AlC	V_2AlC VO_2 V_2O_5	VO_2 V_2O_5 V_3O_5 AlV_2O_4* AlV_3O_9*		
30	V_2AlC	V_2AlC	V_2AlC VO_2 V_2O_5	VO_2 V_2O_5 V_3O_5 AlV_2O_4* AlV_3O_9*		

* Metastable phases.

collected intensities are fairly low leading to the assumption that longer oxidation times would allow the phase to decompose completely. The SEM observations (Fig. 2 (b) and (c)) are consistent with observations made by Gupta and Barsoum and Wang et al. [28,29] Table 1 summarizes the indexed phases with respect to oxidation time and

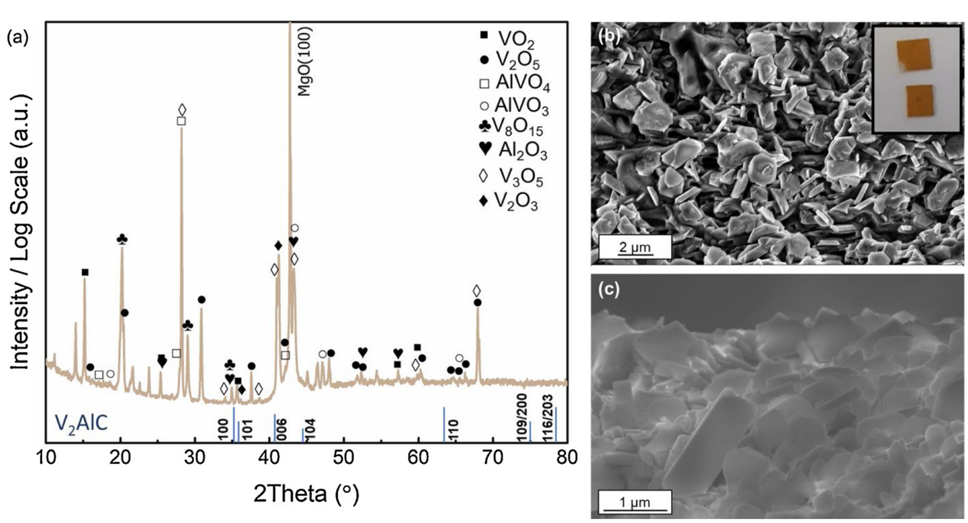

Fig. 2. (a) XRD pattern of the coating oxidised for 5 min at 800 ˚C. SEM micrographs of (b) the surface and (c) the cross-section of the coating. The inset in (b) displays a photograph of sample appearances.

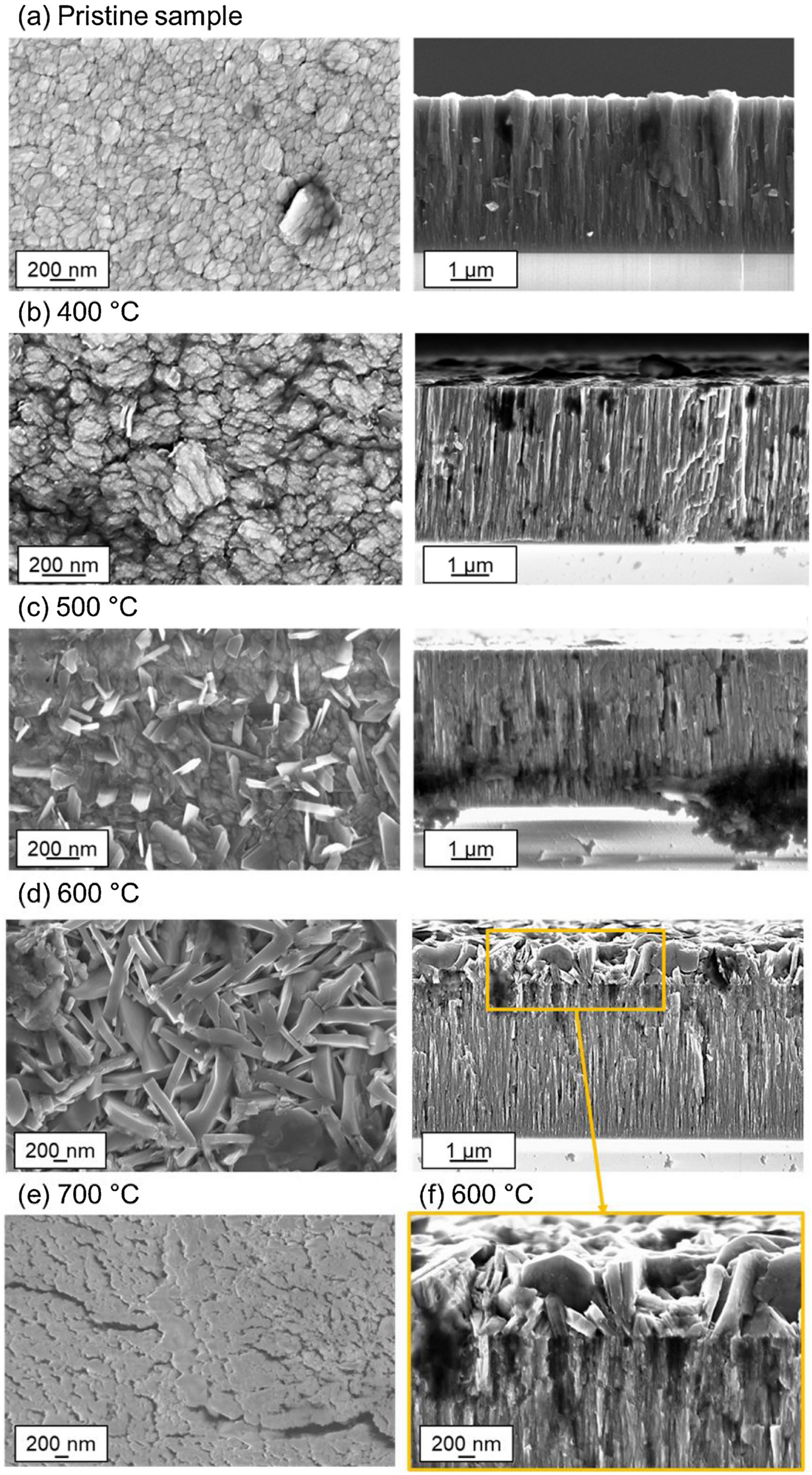

Fig. 3. Representative SEM micrographs of surface and cross-sections of (a) the pristine coating and those oxidised for 30 min at (b) 400, (c) 500, (d), (f) 600, and (e) 700 °C. The cross-section of the coating at 700 °C delaminated and is therefore not displayed.

temperature for the coatings shown in Figs. 1 and 2. Interestingly, a similar behaviour has been observed for Mo_2Ga_2C, which is ternary carbide phase similar to MAX phases. Indeed, oxidation has been observed at temperatures as low as 600 and 700 °C resulting in the coexistence of the Mo_2Ga_2C phase and MoO_3. However, at 800 °C, the oxidation product is no longer MoO_3 but rather Ga_2O_3. Similar microstructural observations have also been observed. [41]

The SEM micrographs of the surfaces and cross-sections of the pristine coating and the samples oxidised for 30 min up to 700 °C are given in Fig. 3. The pristine sample (Fig. 3 (a)) exhibits a columnar microstructure and a rough surface constituted of longitudinal grains of 100–150 nm in size. The column boundaries seem to be under-dense which may lead to a rapid oxidation as boundaries often facilitate inward O diffusion. The density of the coatings was determined through XRR and was calculated to be around 4.26 g/cm^3 and, hence, 13 % lower than the calculated density of 4.87 g/cm^3 as reported in [42]. Similar observations were made for the coating in Fig. 3 (b), although pores have appeared, indicating that diffusion commences at temperatures as low as 400 °C. The first microstructural variations can be observed at 500 °C, where V-rich flakes can be seen to grow out of the surface. Furthermore, the increase in porosity can also be noticed in the cross-section Fig. 3 (c) although the coating thickness remains fairly constant. At 600 °C, catastrophic oxidation is triggered. In fact, the surface shown in Fig. 3 (d) is mostly composed of rectangular grains, which have grown on top of the porous MAX phase coating, as seen from the cross-section. A higher magnification of the area given by the orange square is shown in Fig. 3 (f), where a ~ 1 μm-thick scale on top of the original coating can be observed. Finally, at 700 °C, the coating has cracked and is partially delaminated due to rapid cooling. It is difficult to distinguish the grains, except for some obvious and nicely-shaped crystals, as seen in Fig. 3 (e). The rough features compare favourably with observations made by Wang et al. on an oxidised bulk sample at 650 °C [29].

Fig. 4 shows the electrical resistivity variation of the pristine and oxidised coatings with respect to oxidation time for temperatures up to 600 °C. Resistivity measurements allowed to track the oxidation behaviour of the V_2AlC MAX phase coating. [32,43] The resistivity of the coatings oxidised at 400 °C for all oxidation times do not vary particularly indicating that the metallic character of the MAX phase is still intact. However, at 500 °C, the resistivity increases slightly signifying that at least the surface has changed. At 600 °C, the resistivity increases significantly led by a more advanced oxidation level of the coatings. Indeed, the highest resistivity was observed after 30 min oxidation and a resulting oxide scale of ~ 1 μm. The coatings oxidised at 700 and 800 °C are not presented, as measurements could not be carried out because the coatings were too insulating.

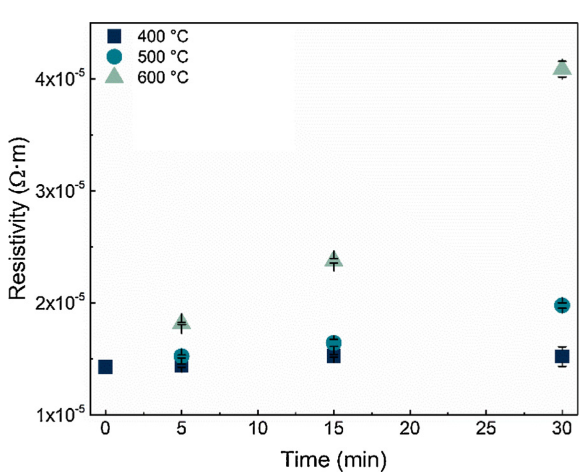

Fig. 4. Electrical resistivity measured on the pristine and oxidised coatings from 400 to 600 °C with respect to oxidation time. Error bars were deduced from sets of 3 measurements.

The elemental composition of the pristine coating as well as those of the coatings oxidised for 5 min at 600 and 800 °C were determined using ERDA, which further allowed determining the composition profiles of each coating. Using the measured density of 4.26 g/cm^3 and the atomic masses of V, Al, C and O depth profile of 2500 × 10^{15} atoms/cm^2 corresponds to a thickness of approximately 325 nm from the surface. The composition profiles are given in Fig. 5, while the average compositions of the coatings are given in Table 2. The pristine sample exhibits the expected 2:1:1 composition of the MAX phase with O contents of approximately 8 at.% throughout the thickness of the analysed area. This O content is related to the low density of the pristine coating. The composition profile of the coating oxidised at 600 °C shows that O is now predominant, whereas the surface is V-rich and Al-depleted, indicating that amorphous Al_2O_3 was not formed (zone 1 in Fig. 5 (b)). However, at a depth of approximately 190 nm the V and Al contents become equal at approximately 22 at.% (zone 2 in Fig. 5 (b) and Table 2). At 800 °C, C is almost completely consumed, and the coating is mostly composed of V- and Al-based oxides. The compositions of the coatings can be tracked in Table 2, where the decrease of C content and increase of O with respect to the oxidation temperature can be noticed. Furthermore, an unusual behaviour of Al at 600 °C can be observed. Indeed, the average Al content throughout the analysed depth profile was approximately 13 at.% at 600 °C, while at 800 °C the content was 22 at.%. Therefore, the loss of Al at 600 °C is most likely caused by sublimation. Furthermore, O has been shown to preferentially replace C vacancies in V_2AlC. In fact, to Baben et al. have conducted calculations to predict the O incorporation in selected M_2AlC MAX phases [44]. In the case of Cr_2AlC, for example, the O tends to replace Al vacancies leading to the nucleation of Al_2O_3. However, O tends to replace C vacancies in the case of V_2AlC and Ti_2AlC, hence promoting the nucleation of V- and Ti-based oxides. This conclusion is consistent with the observations made in this study as the O content increase is concurrent with a significant C content decrease. Therefore, Al is not bound to O or to the MAX phase and can sublimate freely. It is only at higher temperatures and therefore, at higher O contents, that Al_2O_3 nucleates either due to more rapid O diffusion and/or due to the decomposition of metastable Al-containing ternary oxides.

In order to confirm the ERDA observations and further the investigation on the behaviour of Al at high temperatures, XPS was carried out to analyse the surface chemistry of the pristine coating and the one oxidised 600 °C for 5 min. The corresponding sets of V 2p, Al 2p, C 1s, and O 1s spectra are shown in Figs. 6 and 7, respectively. Spectra are presented as a function of sputter time.

After the first sputtering cycle, the V 2p spectra from pristine sample (Fig. 6(a)) becomes characteristic of V—C with the $2p_{3/2}$ component at 513.0 eV [45]. The Al 2p spectra shows two contributions: a narrow peak at 72.8 and a broader signal at ~75.2 eV which are assigned to Al-Al and Al-O, respectively [46]. In contrast to V 2p spectra, the Al-oxide component is present even at larger depths. This is consistent with the evolution of the O 1s spectra (Fig. 6(d)), which shows a single peak at 532.0 eV due to Al-O bond, [45] indicating that the O is present deeper in the coating. The C 1s spectra in Fig. 6(c) reveals three peaks at 282.5, 285.2, and 289.2 eV due to carbide (C-Al/C-V), C-C/C-H, and O-C=O bonding. [47] The latter peaks are characteristic of adventitious C that accumulates on all surfaces. While the carbon-oxide species disappear after the first sputter cycle, the C-C/C-H component persists much deeper into the coating and eventually disappears after the last sputter cycle. This can indicate a certain degree of porosity which allows for accumulation of C-containing species along column boundaries and O penetration which eventually leads to the Al-oxide formation. The above observations are consistent with the ERDA composition profiles which also indicate significant O contents at larger depths.

The surface chemistry differs essentially for the coating oxidised at 600 °C (see Fig. 7). V 2p spectra reveals the presence of two chemical states for V atoms: V-O and V-V with the relative contribution of the

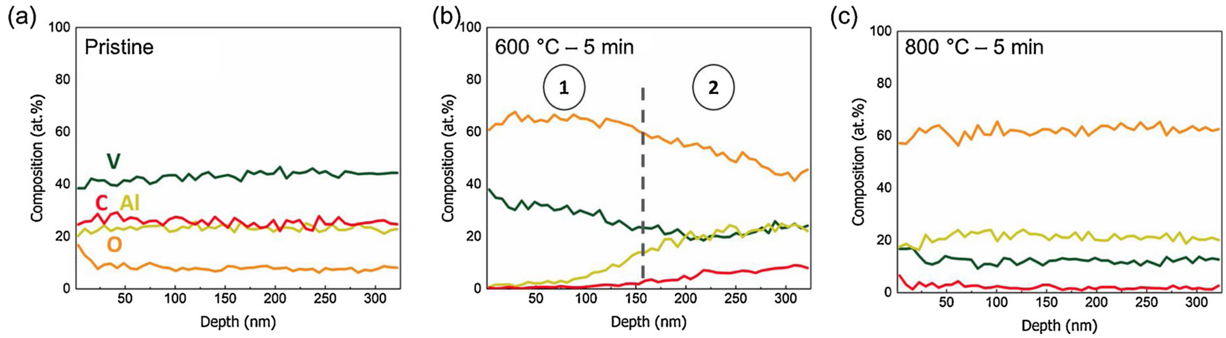

Fig. 5. ERDA depth profiles of (a) the pristine coating, (b) the coating oxidised at 600 °C for 5 min and (c) the coating oxidised at 800 °C for 5 min, to a depth of approximately 325 nm from the surface.

Table 2
Average compositions of coatings determined by ERDA, excluding the surface-near region.

Sample	V (at.%)	Al (at.%)	O (at.%)	Mg (at.%)	C (at.%)
Pristine	44.8 ± 0.2	24.0 ± 0.2	8.1 ± 0.1	–	23.0 ± 0.2
600 °C - 5 min (zone 1)	28.9 ± 0.7	4.9 ± 0.5	64.9 ± 0.4	0.5 ± 0.04	1.0 ± 0.1
600 °C - 5 min (zone 2)	21.7 ± 0.4	22.4 ± 0.8	49.4 ± 1.2	0.3 ± 0.03	6.1 ± 0.4
800 °C - 5 min	12.1 ± 0.2	21.5 ± 0.2	62.4 ± 0.3	2.4 ± 0.1	1.7 ± 0.1

latter one increasing with sputter depth. This is fully consistent with the O 1s spectra, which exhibit one broad peak at all depths centred at 531.0 eV, i.e., at 1 eV lower binding energy than in the case of the pristine sample, which confirms that a different type of oxide, namely V-O, forms in this case. Al 2p spectra (Fig. 7 (b)) shows that almost no Al is present in the surface region, supporting the hypothesis of Al sublimation. Similarly, C is only present at the very surface as C-C/C-H, C-O, and O-C = O, while no carbide peak is observed at any depth. Hence, XPS results are, here as well, consistent with ERDA analyses confirming that the outer surface of the coating oxidised at 600 °C is vanadium oxide rich.

Finally, in order to visualise the presence of the different species within the thickness of the coating after 5 min at 600 °C, STEM imaging was carried out on a FIB lamella and allowed for qualitative elemental analysis throughout the entire coating thickness. Micrographs were obtained in bright field and high angle annular dark field (HAADF) modes and are shown in Fig. 8 (a) and (b), respectively. In addition, EDX line scans are provided with and without O and are shown in Fig. 8 (c) and (d) since the K-shell transition of O and the L-shell transition of V at 0.525 keV and 0.511 keV are very similar. First one can notice the chemical contrast observed at the surface of the coating which is directly related to the V-rich oxides that were formed. In Fig. 8 (d) one can notice the V-rich peak at the outer surface of the coating, right after that peak, however, the Al content rises quite significantly up to approximately 45 at.% over a range of 100 − 200 nm before returning to its original composition. Over this same range, there is a depletion of V. In agreement with the ERDA depth profile shown in Fig. 5 (b), it seems that Al is concentrated below the vanadium oxides, indicating that the

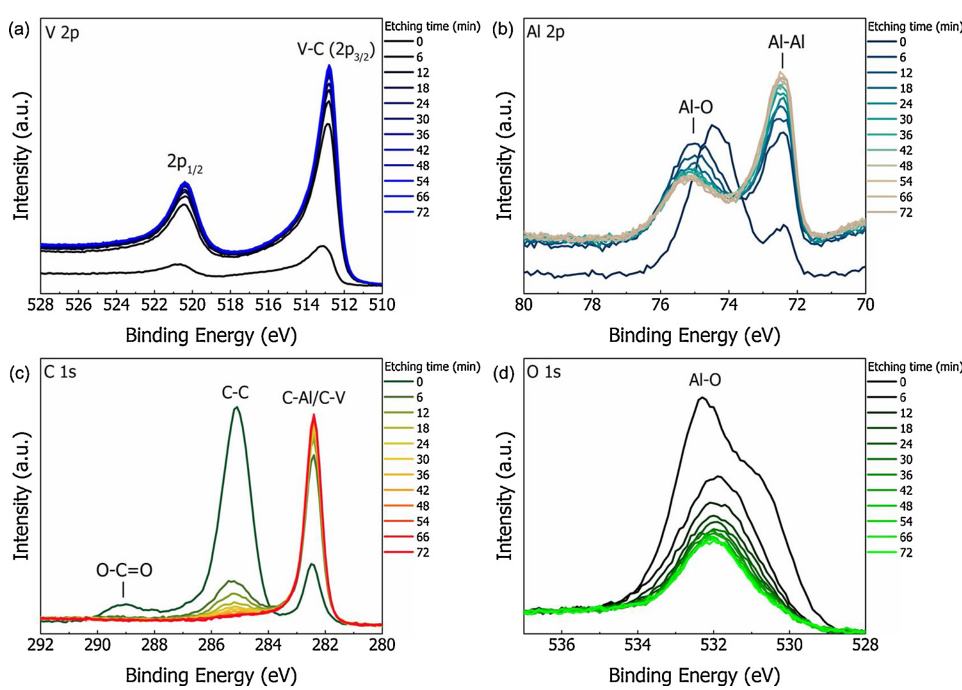

Fig. 6. (a) V 2p, (b) Al 2p, (c) C 1s, and (d) O 1s spectra obtained from a pristine V_2AlC coating as a function of sputter time.

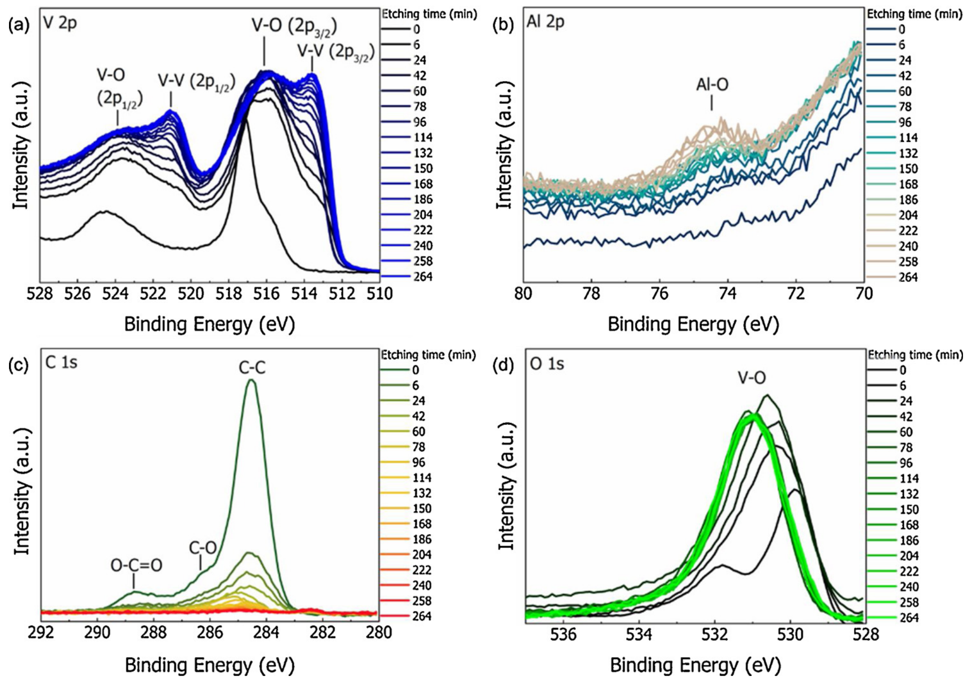

Fig. 7. (a) V 2p, (b) Al 2p, (c) C 1s, and (d) O 1s spectra obtained from a V_2AlC coating oxidised at 600 °C for 5 min as a function of sputter time.

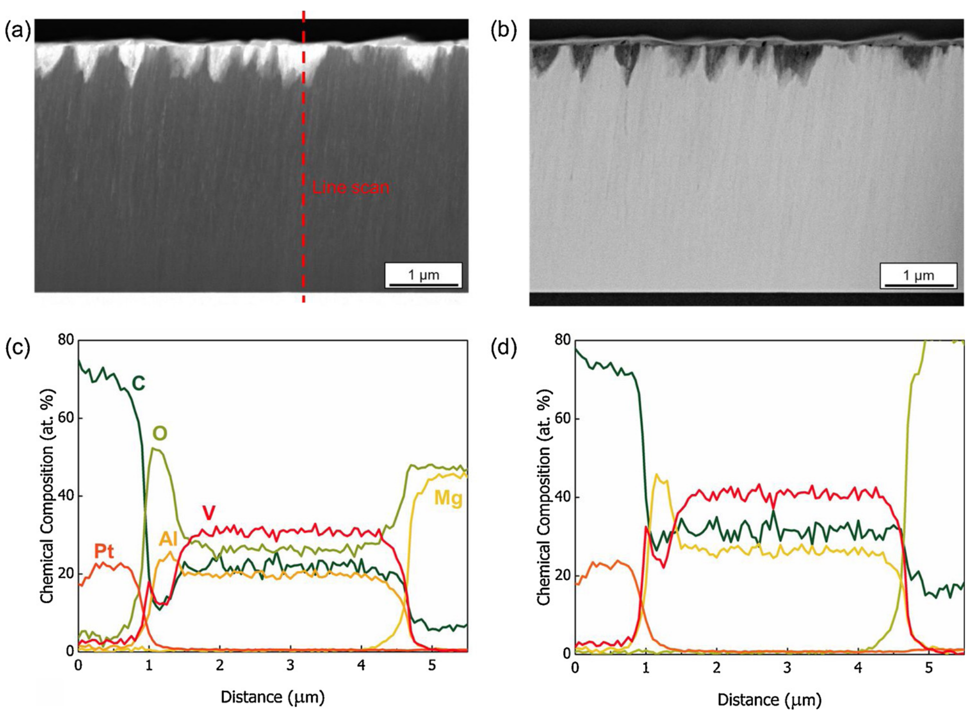

Fig. 8. (a) Bright field and (b) HAADF STEM micrographs of the coating oxidised for 5 min at 600 °C. Top and bottom regions correspond to a Pt protection layer for FIB lift-out as well as the MgO substrate. (c) EDX concentration profiles of the cross-section of the coating with oxygen and (d) without oxygen (region of the line scan shown in (a)).

outward diffusion of V is faster than that of Al.

4. Conclusions

This work is focused on understanding the oxidation behaviour of V_2AlC MAX coatings. Phase pure V_2AlC was deposited at 580 °C from a powder metallurgical composite target and did not require further annealing. The pristine coating was shown to be under-dense as evidenced by XRR measurements and O contents within the coatings. The oxidation behaviour of the coatings after short times at temperatures comprised between 400 and 800 °C, in air, was investigated. The first microstructural change was observed after 15 min at 500 °C, where V-rich flake-like features grew on the surface. The first secondary phase contribution observed through XRD was seen after 5 min at 600 °C and was indexed as VO_2. Microstructural observations at 600 °C have shown that V-rich grains grew on top of the coating, proving the outward diffusion of V species. While V contributions were evidenced both through XRD and EDS analyses, little information could be found on Al. ERDA profiles and XPS core-level analyses have shown that at 600 °C, most of the oxides observed are V-based, while the coatings are Al-depleted. No evidence of the formation of amorphous Al_2O_3 could be obtained at this temperature. However, XPS data are consistent with the notion of Al sublimation at intermediate temperatures. From ERDA measurements on the coating oxidised at 800 °C, and XRD, α-Al_2O_3 and $AlVO_4$ are formed either by more rapid O diffusion, and subsequent reaction, or by decomposition of metastable phases. Furthermore, short time oxidation at these temperatures is shown to drastically affect the metallic behaviour of the V_2AlC MAX phases, particularly above 500 °C. In fact, the V_2AlC MAX phase is self-reporting its degradation by tracking the oxidation progress of the coating via ex-situ electrical resistivity measurements.

Declaration of Competing Interest

The authors declare that they have no known competing financial interests or personal relationships that could have appeared to influence the work reported in this paper.

Acknowledgements

The authors acknowledge funding from the Euratom research and training programme 2014–2018 under grant agreement No. 740415 (H2020 IL TROVATORE), the Swedish Government Strategic Research Area in Materials Science on Functional Materials at Linköping University (Faculty Grant SFO-Mat-LiU No. 2009 00971), and the Foundation Olle Engkvist Byggmästare, grant no. 184-561. The authors also acknowledge financial support from the Swedish research council, VR-RFI (contracts #821-2012-5144 & #2017-00646_9), and the Swedish Foundation for Strategic Research (SSF, contract RIF14-0053) supporting the operation of the tandem accelerator at Uppsala University. GG acknowledges financial support from Swedish Research Council VR Grant 2018-03957 and the VINNOVA grant 2019-04882. CA acknowledges support from the International Union for Vacuum Science, Technique and Applications through the Medard W. Welch International Scholarship 2019.

References

[1] M.W. Barsoum, MN+1AXN phases: a new class of solids; Thermodynamically stable nanolaminates, Prog. Solid State Chem. 28 (2000) 201–281, https://doi.org/10.1016/S0079-6786(00)00006-6.
[2] M.W. Barsoum, T. El-Raghy, The MAX phases: unique new carbide and nitride materials: tertiary ceramics are soft and machinable, yet heat-tolerant, strong and lighweight, Am. Sci. 89 (2001) 334–343, https://doi.org/10.1511/2001.4.334.
[3] M. Radovic, M.W. Barsoum, MAX phases: bridging the gap between metals and ceramics, Am. Ceram. Soc. Bull. 92 (2013) 20–27.
[4] P. Eklund, M. Beckers, U. Jansson, H. Högberg, L. Hultman, The Mn + 1AXn phases: materials science and thin-film processing, Thin Solid Films. 518 (2010) 1851–1878, https://doi.org/10.1016/j.tsf.2009.07.184.
[5] C. Wang, T. Yang, J. Xiao, S. Liu, J. Xue, Q. Huang, J. Zhang, J. Wang, Y. Wang, Structural transitions induced by ion irradiation in V2AlC and Cr2AlC, J. Am. Ceram. Soc. 99 (2016) 1769–1777, https://doi.org/10.1111/jace.14118.
[6] D.J. Tallman, B. Anasori, M.W. Barsoum, A critical review of the oxidation of Ti2AlC, Ti3AlC2 and Cr2AlC in air, Mater. Res. Lett. 1 (2013) 115–125, https://doi.org/10.1080/21663831.2013.806364.
[7] I.M. Low, An overview of parameters controlling the decomposition and degradation of Ti-based M n+1 AX n phases, Materials (Basel). 12 (2019) 1–12, https://doi.org/10.3390/ma12030473.
[8] J. Frodelius, J. Lu, J. Jensen, D. Paul, L. Hultman, P. Eklund, Phase stability and initial low-temperature oxidation mechanism of Ti 2AlC thin films, J. Eur. Ceram. Soc. 33 (2013) 375–382, https://doi.org/10.1016/j.jeurceramsoc.2012.09.003.
[9] I.M. Low, W.K. Pang, Thermal stability of MAX phases, Key Eng. Mater. 617 (2014) 153–158, https://doi.org/10.4028/www.scientific.net/KEM.617.153.
[10] W.K. Pang, I.M. Low, B.H. O'Connor, A.J. Studer, V.K. Peterson, Z.M. Sun, J.P. Palmquist, Comparison of thermal stability in MAX211 and 312 phases, J. Phys. Conf. Ser. 251 (2010), https://doi.org/10.1088/1742-6596/251/1/012025.
[11] D.E. Hajas, M. Scholz, S. Ershov, B. Hallstedt, J.-P. Palmquist, J.M. Schneider, Thermal and chemical stability of Cr2AlC in contact with a-Al2O3 and NiAl, Int. J. Mater. Res. 101 (2010) 1519–1523, https://doi.org/10.3139/146.110439.
[12] B. Hallstedt, D. Music, Z. Sun, Thermodynamic evaluation of the Al-Cr-C system, zeitschrift fuer met, Res. Adv. Tech. (2006), https://doi.org/10.3139/146.101270.
[13] L.O. Xiao, S.B. Li, G. Song, W.G. Sloof, Synthesis and thermal stability of Cr2AlC, J. Eur. Ceram. Soc. 31 (2011) 1497–1502, https://doi.org/10.1016/j.jeurceramsoc.2011.01.009.
[14] S.R. Kulkarni, M. Merlini, N. Phatak, S.K. Saxena, G. Artioli, S. Gupta, M.W. Barsoum, High-temperature thermal expansion and stability of V2AlC Up to 950°C, J. Am. Ceram. Soc. 90 (2007) 3013–3016, https://doi.org/10.1111/j.1551-2916.2007.01847.x.
[15] Y. Jiang, R. Iskandar, M.T. Baben, T. Takahashi, J. Zhang, J. Emmerlich, J. Mayer, C. Polzer, P. Polcik, J.M. Schneider, Growth and thermal stability of (V,Al)2Cx thin films, J. Mater. Res. 27 (2012) 2511–2519, https://doi.org/10.1557/jmr.2012.202.
[16] S. Mráz, M. Tyra, M. to Baben, M. Hans, X. Chen, F. Herrig, K. Lambrinou, J.M. Schneider, Thermal stability enhancement of Cr2AlC coatings on Zr by utilizing a double layer diffusion barrier, J. Eur. Ceram. Soc. 40 (2020) 1119–1124, https://doi.org/10.1016/j.jeurceramsoc.2019.10.008.
[17] K.G. Pradeep, K. Chang, A. Kovács, S. Sen, A. Marshal, R. de Kloe, R.E. Dunin-Borkowski, J.M. Schneider, Nano-scale Si segregation and precipitation in Cr 2 Al (Si)C MAX phase coatings impeding grain growth during oxidation, Mater. Res. Lett. 7 (2019) 180–187, https://doi.org/10.1080/21663831.2019.1572663.
[18] D.B. Lee, T.D. Nguyen, Cyclic oxidation of Cr2AlC between 1000 and 1300 °C in air, J. Alloys Compd. 464 (2008) 434–439, https://doi.org/10.1016/j.jallcom.2007.10.018.
[19] W. Tian, P. Wang, Y. Kan, G. Zhang, Oxidation behavior of Cr2AlC ceramics at 1,100 and 1,250 °c, J. Mater. Sci. 43 (2008) 2785–2791, https://doi.org/10.1007/s10853-008-2516-2.
[20] D.B. Lee, S.W. Park, Oxidation of Cr 2AlC between 900 and 1200 °C in air, Oxid. Met. 68 (2007) 211–222, https://doi.org/10.1007/s11085-007-9071-0.
[21] D.B. Lee, T.D. Nguyen, J.H. Han, S.W. Park, Oxidation of Cr2AlC at 1300 °C in air, Corros. Sci. 49 (2007) 3926–3934, https://doi.org/10.1016/j.corsci.2007.03.044.
[22] D.E. Hajas, M. To Baben, B. Hallstedt, R. Iskandar, J. Mayer, J.M. Schneider, Oxidation of Cr2AlC coatings in the temperature range of 1230 to 1410°C, Surf. Coatings Technol. 206 (2011) 591–598, https://doi.org/10.1016/j.surfcoat.2011.03.086.
[23] D.B. Lee, T.D. Nguyen, S.W. Park, Long-time oxidation of Cr2AlC between 700 and 1,000 °c in air, Oxid. Met. 77 (2012) 275–287, https://doi.org/10.1007/s11085-012-9285-7.
[24] J. Wang, Y. Zhou, T. Liao, J. Zhang, Z. Lin, A first-principles investigation of the phase stability of Ti 2 AlC with Al vacancies, Scr. Mater. 58 (2008) 227–230, https://doi.org/10.1016/j.scriptamat.2007.09.048.
[25] B. Cui, D.D. Jayaseelan, W.E. Lee, TEM study of the early stages of Ti 2AlC oxidation at 900 °c, Scr. Mater. 67 (2012) 830–833, https://doi.org/10.1016/j.scriptamat.2012.07.045.
[26] L. Xu, D. Zhu, Y. Liu, T.S. Suzuki, B. nam Kim, Y. Sakka, S. Grasso, C. Hu, Effect of texture on oxidation resistance of Ti3AlC2, J. Eur. Ceram. Soc. 38 (2018) 3417–3423, https://doi.org/10.1016/j.jeurceramsoc.2018.03.009.
[27] W. Yu, M. Vallet, B. Levraut, V. Gauthier-Brunet, S. Dubois, Oxidation mechanisms in bulk Ti2AlC: influence of the grain size, J. Eur. Ceram. Soc. (2020), https://doi.org/10.1016/j.jeurceramsoc.2020.01.042.
[28] S. Gupta, M.W. Barsoum, Synthesis and oxidation of V2AlC and (Ti0.5, v 0.5)2AlC in air, J. Electrochem. Soc. 151 (2004) 24–29, https://doi.org/10.1149/1.1639160.
[29] B. Wang, A. Zhou, Q. Hu, L. Wang, Synthesis and oxidation resistance of V2AlC powders by molten salt method, Int. J. Appl. Ceram. Technol. 14 (2017) 873–879, https://doi.org/10.1111/ijac.12723.
[30] Y. Zhang, H.J. Whitlow, T. Winzell, I.F. Bubb, T. Sajavaara, K. Arstila, J. Keinonen, Detection efficiency of time-of-flight energy elastic recoil detection analysis systems, Nucl. Instruments Methods Phys. Res. Sect. B Beam Interact. with Mater. Atoms. 149 (1999) 477–489, https://doi.org/10.1016/S0168-583X(98)00963-X.
[31] J.M. Janson, CONTES (Conversion of Time-Energy Spectra), a Program for ERDA Data Analysis, Intern. Report, Uppsala Univ., 2004.
[32] B. Stelzer, X. Chen, P. Bliem, M. Hans, B. Völker, R. Sahu, C. Scheu, D. Primetzhofer, J.M. Schneider, Remote tracking of phase changes in Cr2AlC thin films by in-situ resistivity measurements, Sci. Rep. 9 (2019) 1–7, https://doi.org/10.1038/s41598-019-44692-4.
[33] G. Greczynski, L. Hultman, Compromising science by ignorant instrument calibration—need to revisit half a century of published XPS data, Angew. Chemie Int. Ed. (2020), https://doi.org/10.1002/anie.201916000.
[34] G. Greczynski, L. Hultman, C 1s Peak of adventitious carbon aligns to the vacuum level: Dire consequences for material's bonding assignment by photoelectron spectroscopy, ChemPhysChem. (2017), https://doi.org/10.1002/cphc.201700126.
[35] G. Greczynski, D. Primetzhofer, J. Lu, L. Hultman, Core-level spectra and binding energies of transition metal nitrides by non-destructive x-ray photoelectron spectroscopy through capping layers, Appl. Surf. Sci. 396 (2017) 347–358, https://doi.org/10.1016/j.apsusc.2016.10.152.
[36] E. Lewin, J. Counsell, J. Patscheider, Spectral artefacts post sputter-etching and how to cope with them – a case study of XPS on nitride-based coatings using monoatomic and cluster ion beams, Appl. Surf. Sci. 442 (2018) 487–500, https://doi.org/10.1016/j.apsusc.2018.02.191.
[37] T. Reeswinkel, D. Music, J.M. Schneider, Ab initio calculations of the structure and mechanical properties of vanadium oxides, J. Phys. Condens. Matter. 21 (2009), https://doi.org/10.1088/0953-8984/21/14/145404.
[38] V. Brázdová, M.V. Ganduglia-Pirovano, J. Sauer, Crystal structure and vibrational spectra of AlVO4, A DFT study, J. Phys. Chem. B. 109 (2005) 394–400, https://doi.org/10.1021/jp046055v.
[39] B. Reuter, R. Aust, G. Colsmann, C. Neuwald, Darstellung und eigenschaften vanadium(II)-haltiger und damit n-leitender vanadium(III)-spinelle, Zeitschrift Fuer Anorg, Und Allg. Chemie. 500 (1983) 188–198.
[40] G. Yang, H. Song, G. Yang, M. Wu, C. Wang, 3D hierarchical AlV3O9 microspheres: first synthesis, excellent lithium ion cathode properties, and investigation of electrochemical mechanism, Nano Energy. 15 (2015) 281–292, https://doi.org/10.1016/j.nanoen.2015.04.038.
[41] H. He, S. Jin, G. Fan, L. Wang, Q. Hu, A. Zhou, Synthesis mechanisms and thermal stability of ternary carbide Mo2Ga2C, Ceram. Int. 44 (2018) 22289–22296, https://doi.org/10.1016/j.ceramint.2018.08.353.
[42] J. Etzkorn, M. Ade, H. Hillebrecht, V2AlC, V4AlC3-x (x ≈ 0.31), and V 12Al3C8: synthesis, crystal growth, structure, and superstructure, Inorg. Chem. 46 (2007)

7646–7653, https://doi.org/10.1021/ic700382y.
[43] B. Stelzer, M. Momma, J.M. Schneider, Autonomously Self-Reporting Hard Coatings: Tracking the Temporal Oxidation Behavior of TiN by In Situ Sheet Resistance Measurements, Adv. Funct. Mater. 30 (2020) 1–5, https://doi.org/10.1002/adfm.202000146.
[44] M. Baben, L. Shang, J. Emmerlich, J.M. Schneider, Oxygen incorporation in M 2AlC (M = Ti, V, Cr), Acta Mater. 60 (2012) 4810–4818, https://doi.org/10.1016/j.actamat.2012.05.011.
[45] G. Greczynski, D. Primetzhofer, L. Hultman, Reference binding energies of transition metal carbides by core-level x-ray photoelectron spectroscopy free from Ar + etching artefacts, Appl. Surf. Sci. 436 (2018) 102–110, https://doi.org/10.1016/j.apsusc.2017.11.264.
[46] G. Greczynski, L. Hultman, M. Odén, X-ray photoelectron spectroscopy studies of Ti1-xAlxN (0 ≤ x ≤ 0.83) high-temperature oxidation: the crucial role of Al concentration, Surf. Coatings Technol. 374 (2019) 923–934, https://doi.org/10.1016/j.surfcoat.2019.06.081.
[47] G. Greczynski, S. Mráz, L. Hultman, J.M. Schneider, Venting temperature determines surface chemistry of magnetron sputtered TiN films, Appl. Phys. Lett. (2016), https://doi.org/10.1063/1.4940974.